journal of the mechanical behavior of biomedical materials 106 (2020) 103749

Contents lists available at ScienceDirect

Journal of the Mechanical Behavior of Biomedical Materials

journal homepage: http://www.elsevier.com/locate/jmbbm

Structural, chemical and optical characterizations of an experimental SiO_2–Y-TZP ceramic produced by the uniaxial/isostatic pressing technique

Victor Mosquim [a], Brunna Mota Ferrairo [b], Mariele Vertuan [a], Aroldo Geraldo Magdalena [c], Carlos Alberto Fortulan [d], Paulo Noronha Lisboa-Filho [e], Paulo Francisco Cesar [f], Estevam Augusto Bonfante [b], Heitor Marques Honório [g], Ana Flávia Sanches Borges [a,*]

[a] Department of Operative Dentistry, Endodontics and Dental Materials, Bauru School of Dentistry, University of São Paulo, Bauru, SP, Brazil
[b] Department of Prosthodontics and Periodontics, Bauru School of Dentistry, University of São Paulo, Bauru, SP, Brazil
[c] Department of Chemistry, UNESP-School of Science, São Paulo State University, Bauru, SP, Brazil
[d] Department of Mechanical Engineering, São Carlos School of Engineering, University of São Paulo, São Carlos, SP, Brazil
[e] Department of Physics, UNESP-School of Science, São Paulo State University, Bauru, SP, Brazil
[f] Department of Biomaterials and Oral Biology, School of Dentistry, University of São Paulo, São Paulo, SP, Brazil
[g] Department of Pediatric Dentistry, Orthodontics and Public Health, Bauru School of Dentistry, University of São Paulo, Bauru, SP, Brazil

ARTICLE INFO

Keywords:
Electron microscopy (B)
X-ray methods (B)
SiO_2 (D)

ABSTRACT

This study aimed to produce a new SiO_2+Y-TZP ceramic via uniaxial/isostatic compression that was structurally and chemically characterized relating to its translucency and flexural strength. SiO_2 and Y-TZP were mixed using a ball mill, pressed and sintered at 1150 °C. The optical and mechanical properties of the specimens were compared to lithium disilicate (LD) and zirconia-reinforced lithium silicate (ZLS) (Kruskal-Wallis, $\alpha = 0.05$). The Fourier Transform Infrared Spectroscopy bands suggested an interaction between Si, O and Zr. Contrast ratio and translucency parameter of the experimental ceramic were higher and lower, ($p = 0.000001$) respectively, than those of the LD and ZLS. The experimental ceramic presented similar flexural strength to ZLS, but lower than LD ($p < 0.0001$). It can be concluded that this processing method is efficient to obtain a SiO_2+Y-TZP ceramic and 1150 °C crystallizes SiO_2 without inducing *t-m* transformation. The SiO_2+Y-TZP ceramic presented lower translucency and higher masking ability than the commercially available glass-ceramics, but similar flexural strength to one glass-ceramics.

1. Introduction

Dental ceramics are used as restorative materials due to their inherited properties, such as the color stability, resistance to wear, high strength, biocompatibility and low biofilm accumulation (Kelly and Benetti, 2011; Kelly, 2008). Polycrystalline ceramics, such as zirconia (ZrO_2), own a much higher fracture toughness than glass ceramics, which in turn are more translucent and esthetically appealing. These characteristics are important to be taken into consideration depending on the area these materials are being indicated by the dental practitioner.

In glass ceramics, silicon oxide (SiO_2) is often present (Kelly and Benetti, 2011; Kelly, 2008), and, as an attempt to enhance the mechanical properties of glass ceramics, crystalline materials, such as ZrO_2, are used in these materials (Kelly and Benetti, 2011; Kelly, 2008; Riquieri et al., 2018). Zirconia can be found at three allotropic phases: monoclinic (m), tetragonal (t) and cubic (c). Under room temperature until 1,170 °C the monoclinic phase can be seen. From 1170 until 2,370 °C ZrO_2 is in its tetragonal form, and above that temperature, in cubic form (Chavalier et al., 2007; Kelly and Denry, 2008; El-Gahny and Sherief, 2016). The tetragonal to monoclinic (t-m) transformation result in 4.5% volumetric expansion, which is held responsible for the higher fracture toughness of zirconia. Hence, with the intention to stabilize t-zirconia under room temperature, dopants such as yttrium oxide (Y_2O_3) are used, originating yttria-stabilized tetragonal zirconia (Y-TZP) (Guazzato et al., 2004; Ramos et al., 2015). However, as the zirconia/Y-TZP is known to be opaque, its use in esthetical areas is limited. Therefore, new ceramic materials containing SiO_2 and enriched

* Corresponding author. Department of Operative Dentistry, Endodontics and Dental Materials, Bauru School of Dentistry-FOB-USP, Alameda Octávio Pinheiro Brisolla, 9-75, Bauru, SP, 17012-901, Brazil.
E-mail address: afborges@fob.usp.br (A.F. Sanches Borges).

https://doi.org/10.1016/j.jmbbm.2020.103749
Received 27 November 2019; Received in revised form 19 March 2020; Accepted 24 March 2020
Available online 1 April 2020
1751-6161/

by ZrO_2/Y-TZP has been processed by many different routes, such as sol-gel, slip-casting and uniaxial/isostatic powder compression in order to achieve good optical properties (Mouzon et al., 2008; Jiang et al., 2011; Persson et al., 2012).

The uniaxial/isostatic powder compression technique is a low-cost technique used to produce large amounts of ceramic materials using powders as starting points. This technique is based on applying pressure to a mold so the powder in it can be compressed. Thereafter, this green-body material is submitted to a sintering protocol with an attempt to density the material. Densification is important to reduce porosities, irregularities and internal spaces generated during the fabrication method (Volpato et al., 2011; McCabe et al., 2008), which are also related to the mechanical properties and transmittance of light inside the materials bulk (Jiang et al., 2011). Also, nano-sized powders are used in order to generate more uniform and smoother surfaces, which, associated with proper heating protocols could lead to good mechanical behavior and proper light transmittance, i.e., translucency.

Translucency can be defined as the amount of light that is transmitted or reflected from a materials surface through a turbid medium (Brodbelt et al., 1980). As shown in previous studies (Jiang et al., 2011; Heffernan et al., 2001), the size, the amount of crystals in the material and also its porosity play important roles regarding the amount of light transmitted through the material, consequently interfering in the translucency of a given substrate. For these reasons, high levels of porosities, as well as the amount of crystalline content composing one specific material can lead to light scattering and diffuse reflection of light due to different refractive indices between the matrix, the air inside those pores and the crystals used for enrichment purposes, resulting in low translucency which is seen as undesired opaqueness (Jiang et al., 2011).

Considering these obstacles at reaching proper translucency, the processing methods play an important role at achieving the desired optical properties (Mouzon et al., 2008; Jiang et al., 2011; Persson et al., 2012). Though, these processing methods used to obtain experimental ceramics are not commonly used to create ceramics with dental purposes, justifying the need to structurally characterize the materials produced by them and evaluate their desired properties. Therefore, since new glass ceramics enriched by polycrystalline materials has been produced by different processing methods and achieved interesting results, the aim of this study was to produce a new glass ceramic containing SiO_2+Y-TZP via uniaxial/isostatic powder compression and structurally and chemically characterize this material relating to its mechanical and optical properties.

2. Materials and methods

The materials used in this study were Tetraethyl orthosilicate (TEOS, 99.9%, Sigma-Aldrich, San Luis, Missouri, USA), absolute alcohol (C_2H_5OH, 99.8%), ammonium hydroxide (NH_4OH, 99.9%), Zpex® (Tosoh Corporation, Tokyo, Japan; batch no. Z306234P; surface area of 15.1 m^2/g), which contained Y_2O_3 (5.35 ± 0.2 wt.%), HfO_2 (<5.0 wt.%), Al_2O_3 (≤0.1 wt.%), Na_2O (≤0.04 wt.%), SiO_2 (≤0.02 wt.%), Fe_2O_3 (≤0.01 wt.%), lithium disilicate (LD) CAD/CAM block (IPS e.max CAD®, Ivoclar Vivadent, Schaan, Liechtenstein), zirconia-reinforced lithium silicate (ZLS) CAD/CAM block (Celtra Duo®, Dentsply, York, Pennsylvania, USA).

2.1. Synthesis of silica

The synthesis of silica from TEOS was performed according to the methodology used by Li et al. (2012), from the modified Stöber method. This method consists in adding 10 mL of milli-q water and 4 mL of TEOS to a beaker, which was maintained in an ultrasonic machine for 5 min to allow the emulsion of the reagents. Then, 50 mL of absolute alcohol was dispensed into the beaker, followed by 15 mL of NH_4OH, which were dripped into the solution under magnetic stirring (400 rpm) at 40 °C to allow the hydrolysis and condensation of TEOS. The reaction was maintained for 6 h to obtain the white, amorphous silica suspension.

2.2. Initial characterization

The obtained silica and the powder of partially stabilized polycrystalline tetragonal zirconia (Y-TZP) were morphologically, chemically and structurally analyzed by Scanning Electron Microscope/Energy Dispersive X-ray Spectroscopy (SEM/EDX), by X-ray Diffraction (XRD), by a Electron Microscope (TEM) and by Fourier Transform Infrared Spectroscopy (FTIR).

2.2.1. SEM/EDX

Images were obtained using a JEOL-JSM 5600LV microscope (Tokyo, Japan), which is equipped with an X-ray detector (Voyager, Noran Instruments) and allowed the chemical elements analysis to be conducted by EDX under vacuum and in backscattered electron mode.

2.2.2. TEM

The silica and the Y-TZP powders were observed in TEM (CM200 model, Philips, Amsterdam, Netherlands) with a LaB_6 filament (lanthanum hexaboride) and operated at a maximum voltage of 200 kV.

The size of the particles was measured using the Adobe Photoshop CC 2015 software (Adobe Inc., San José, California, USA).

2.2.3. XRD

The X-ray diffractometer (Shimadzu model XDR 7000, Kyoto, Japan) was used with Cu Kα radiation, angular scan between 10° and 70°, with a scan speed of 2 min^{-1}. New analyses were performed after the synthesis of the experimental ceramic, following the specifications of each method, as follows.

The crystalline phases of the initial Y-TZP powder were identified and the amorphous characteristic of the initial silica powder was validated by XRD. After sintering the experimental ceramic, a sample underwent a XRD analysis as well.

The crystalline phases were identified by comparing the spectra obtained with the standard datasheets of the Joint Committee on Powder Diffraction Standards (JCPDS) using the Crystalographica Search-Match software.

2.2.4. FTIR

The initial Y-TZP powder and the silica powder were placed on an FTIR spectrometer (Shimadzu Corporation, Model IR Prestige 21, Kyoto, Honshu, Japan) attached to a ATR device (Smart Miracle™ containing a diamond plate, Pike Technologies, Madison, Wisconsin, USA). Before each reading, each powder was compressed against the ATR diamond crystal using a micrometric low-pressure clamp (408 psi) to allow optimal contact with it. The transmittance spectra were obtained between 4000 and 450cm^{-1} with 32 scans at 4 cm^{-1}. After sintering, one specimen was taken to the FTIR spectrometer to be analyzed following these same parameters.

2.3. Acquisition of the experimental ceramic (silica + Y-TZP)

The experimental ceramic was obtained using the commercial Zpex® injection powder on a nanometric scale (0.04 μm) and the aforementioned silica powder. This mixture respected a 97:3.0 wt.% ratio (Silica: Y-TZP).

The Y-TZP and silica powders were placed in a polyethylene jug, which was filled with 28.25 g of isopropyl alcohol, 513 g of ZrO_2 spheres and 0.145 g of polyvinyl butyral (PVB). Then the jug was kept in a rotatory mill for 2 h. After that time, 1.305 g of polyvinyl butyral (PVB) diluted into 26.1 g of isopropyl alcohol were inserted into the mixture and the jug was again kept in a rotatory mill for another 10 min.

Thereafter, the contents of the jug were dried and sieved through a 180 μm sieve. The mixture was compacted in a metal device previously

lubricated with oleic acid to obtain cold uniaxial compression bars at 80 MPa. The bars were subjected to isostatic compress at 206 MPa for 1min and then sintered at 1150 °C in a $MoSi_2$ furnace for 2 h, with a heating rate displayed in Fig. 1.

2.4. Theoretical density analysis

After sintering, five specimens of the experimental ceramic were submitted to a theoretical density analysis, which is based on Archimedes's principle. For that, each sample was weighted on an analytical scale (Adventurer Analytical balance, Ohaus, Parsippany, New Jersey, USA) three times: when dried, underwater and after immersed in water for 24 h (damp). Their final density is calculated using the equation (1), where ρsample corresponds to the final density of the sample; m_d to the specimen's mass when dry; m_d to the specimen's mass after immersion in deionized water (damp); m_l to the specimen's mass when measured underwater (disregarding the mass of water); and ρliquid to the density of the deionized water (0.99777) used to immerge the sample.

$$\rho_{sample} = \frac{m_d}{(m_d - m_l)} x \rho_{liquid} \quad (1)$$

2.5. Optical properties tests

2.5.1. Sample acquisition (silica + Y-TZP, IPS e.max CAD® and Celtra Duo®)

Ten bars of the experimental ceramic (silica + Y-TZP), one lithium disilicate C14 HT A1 block and one zirconia-reinforced lithium silicate C14 HT A1 block were stabilized on an Isomet 1000 digital cutting machine (Buehler, LakeBluff, IL, USA). Using a diamond wafering blade (Extec XL12205 High Concentration, Extec Corp., Enfield, Connecticut, USA) at 300 rpm under refrigeration, the specimens were cut into 5 mm wide x 7 mm high and 2 mm thick (n = 10/group).

After cutting, the LD specimens were taken to a furnace (Programat EP3000, Ivoclar Vivadent, Schaan, Liechtenstein) for crystallization according to the manufacturer's recommendations in order to obtain their final mechanical and optical properties.

The optical properties of each material were tested on a CM 3700d spectrophotometer (Konica Minolta, Tokyo, Japan), whose wavelength (400 nm–700 nm with intervals of 10 nm) lies in the visible light spectrum and is emitted by a xenon arc lamp. For this test, each specimen was polished using a semi-automatic polishing machine (Automet, 2000; Buehler, Lake Bluff, IL, USA) with 45, 15, 9, 6, 3 and 1 μm granulated diamond disks (Allied High Tech Products, Rancho Dominguez, CA, USA) with diamond suspensions up to 1 μm. Then, they were positioned in the equipment with the 35 mm^2 side facing the light source. Thus, the ten specimens of each group were analyzed only once, acquiring values following the CIELab* (Commission Internationale de l'Éclairage/International Commission of Illumination) parameter on white background (Yw) and on black background (Yb). From these data, the contrast ratio (CR) and the translucency parameter (TP) were calculated, as performed by Nogueira and Della Bona (Nogueira and Della Bona, 2013), and dos Santos et al. (dos Santos et al., 2017).

The CR corresponds to the property that measures transparency (CR = 0) and opacity (CR = 1) of the material obtained through the ratio between the reflectance of the specimen, both on the black background (Yb) and on the white background (Yw) (Nogueira and Della Bona, 2013; Della Bona et al., 2014), which is given by equation (2):

$$CR = Yb/Yw \quad (2)$$

The masking ability of the material corresponds to the TP. This data was obtained by calculating the color difference (ΔE), which was calculated from the L *, a * and b * parameters of the material on the black and white backgrounds (Nogueira and Della Bona, 2013; Della Bona et al., 2014; Chu et al., 2007). The value of ΔE was calculated from the following equation (3):

$$\Delta E = [(L^*_b - L^*_w)^2 + (a^*_b - a^*_w)^2 + (b^*_b - b^*_w)^2]^{1/2} \quad (3)$$

The subscripts b* (black) and w* (white) correspond to the color of the background on which the specimen was positioned in the spectrophotometer.

2.6. Mechanical properties

Following the standards of ISO 6872:2015, the 3-point bending test (σf) was performed using a 500 N load cell at a constant speed of 0.5 mm/min using an Instron 3342 universal test machine (Instron Co.,

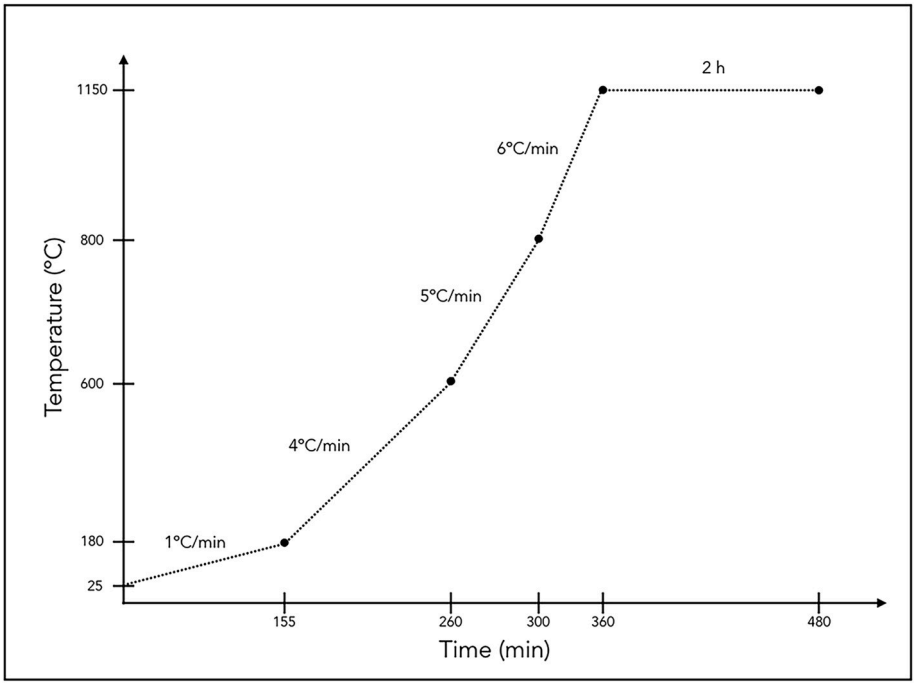

Fig. 1. Heating rate at which the specimens of the experimental group were submitted during sintering.

Canton, MA, USA). For the 3-point bending test, the specimens (n = 10/group) were placed on a metal device, maintaining a distance of 12 mm between the lower cylindrical supports and the load applied at the center of the upper metal rod. During the tests, the bending device was stored submerged in distilled water under a temperature of 37 °C. The values of flexural strength were determined according to equation (4), where P refers to the value of the fracture load in Newtons (N), I refers to the span, which was standardized at 12mm, w refers to the specimen width (approximately 4 ± 0.2 mm) and b refers to the thickness of the specimen (approximately 2.1 ± 1.1 mm).

$$\sigma f = 3Pl / 2wb^2 \quad (4)$$

2.7. Division into groups

For the optical properties analysis, 30 specimens were used in the dimensions of 5 mm wide x 7 mm high and 2 mm thick, totaling 10 specimens for each material (n = 10/group). For the three-point bending test, 30 specimens were used in the dimensions of 4 mm wide x 14 mm high and 2 mm thick, totaling 10 specimens for each material (n = 10/group). The materials were divided into 3 groups, as described in Table 1.

2.8. Statistical analysis

The data regarding the optical and mechanical properties tests were organized on Excel spreadsheets and statistically analyzed using IBM SPSS software (SPSS Inc., Chicago, IL, USA). The normal distribution of data was checked using the Kolmogorov-Smirnov test. As there was no normal distribution to both tests, Kruskal-Wallis followed by post-hoc Dunn tests were applied. All analyses were performed with the level of significance set at 5%.

3. Results

3.1. SEM/EDX

The chemical characterization of Y-TZP and silica was conducted using SEM/EDX. The analysis conducted on silica detected small agglomerations of smaller spherical primary particles of silica (Fig. 2A). Also, the EDX analysis detected silicon (Si) and oxygen (O), in 47.88 wt.% and 52.12 wt.%, respectively (Fig. 2F).

As performed on silica, the Y-TZP powder was also submitted to the same analysis. The SEM analysis indicated several agglomerations of the nano-sized particles (Fig. 2B). The EDX assessment indicated the presence of mainly four chemical elements: zirconium (Zr), oxygen (O) and yttrium (Y) and hafnium (Hf) in 67.06 wt.%, 27.79 wt.%, 4.19 wt.% and 0.95 wt.%, respectively (Fig. 2G).

After sintering, SEM was conducted on a fracture area. In Fig. 2C it is possible to notice the insufficient densification of the sample and the presence of silica grains, characterized by their spherical character. In Fig. 2D–E it can be seen some pores and cracks in the material, which could have functioned as origins of the catastrophic failure.

3.2. TEM

Under TEM analysis, it was possible to confirm that the particles were spherical and amorphous (Fig. 3A, B and 3C). The size of silica particles and their distribution are represented in Fig. 4.

The Y-TZP powder is commercialized in a 40nm scale, therefore a TEM analysis was necessary to properly confirm this statement. Under the TEM analysis, it was possible to observe the heterogeneity of the sample, both in the particles' shape and size (Fig. 3D, E, 3F, 3G).

After mixing the two powder in the determined proportion, the resulting powder was taken to an analysis under TEM. In the acquired images, a particle of Y-TZP can be seen inside the grain of silica (Fig. 3H and I). Also, the amorphous character of silica can be seen due to the lack of a crystallographic pattern, different from Y-TZP, which owns crystallographic patterns, seen in Fig. 3F and G.

3.3. XRD

The structural analysis was conducted by XRD. According to the standard datasheets of the Joint Committee on Powder Diffraction Standards (JCPDS), this structural analysis showed that the silica acquired by the modified Stöber method is amorphous (Fig. 5).

The structural analysis was also performed on the Y-TZP powder. This analysis is expressed in Fig. 5, where more intense peaks are seen in the region of 28, 31 and 35°, attributed to the monoclinic phase of ZrO_2, whilst the ones at 30, 50 and 60° can be attributed to the tetragonal phase. Less intense peaks are also seen at 24, 40, 53, 55 and 62 and are to the monoclinic phase, excepting 55°, which can also be attributed to the tetragonal allotropic phase (Fig. 5) (Hanawalt et al., 1938; Ruff et al., 1929). In this case, unlike what is stated by the manufacturer, the powder is not commercialized solely in its tetragonal form.

The Y-TZP and silica powders were mixed in a ball-mill in the proportions described in the item 2.3 of this paper. Before being submitted to the sintering treatment, it was analyzed structurally. The graph that resulted from this analysis corresponded to an overlapping of the amorphous characteristic attributed to the silica powder and the peaks attributed to the Y-TZP powder. However, the intensity of the peaks detected at 28, 30, 35, 50 and 60° decreased, and the ones located at 53 and 55 could not be seen. Also, the peaks at 24 and 31 were dislocated to 26 and 33°, respectively (Fig. 5). This dislocation can be associated with the formation of $ZrSiO_4$ (Hanawalt et al., 1938).

After sintering at 1150 °C for 2 h, it can be stated that the temperature at which the specimens were sintered was sufficient to crystallize the amorphous silica, once a new peak at the 22° can be seen (Wyckoff, 1925). Also, two delicate new peaks can be seen at 27 and 36°, attributed to the formation of $ZrSiO_4$ (Hanawalt et al., 1938; Liu et al., 2012).

Table 1
Classification and composition of the ceramics used in this study.

GROUP	MATERIAL	CLASSIFICATION	COMPOSITION
EC (Experimental Ceramic)	Experimental ceramic containing silica and Y-TZP nanoparticles	Silica reinforced with 3% of Y-TZP	3% Y-TZP 97% SILICA
LD	IPS e.max CAD®	Lithium disilicate	57–80% SiO_2 11–19% Li_2O 0–13% K_2O 0–11% P_2O_5 0–8% ZrO_2 0–8% ZnO 0–5% Al_2O_3 0–5% MgO
ZLS	Celtra Duo®	Zirconia-reinforced lithium silicate	Lithium silicate with approximately 10% of ZrO_2

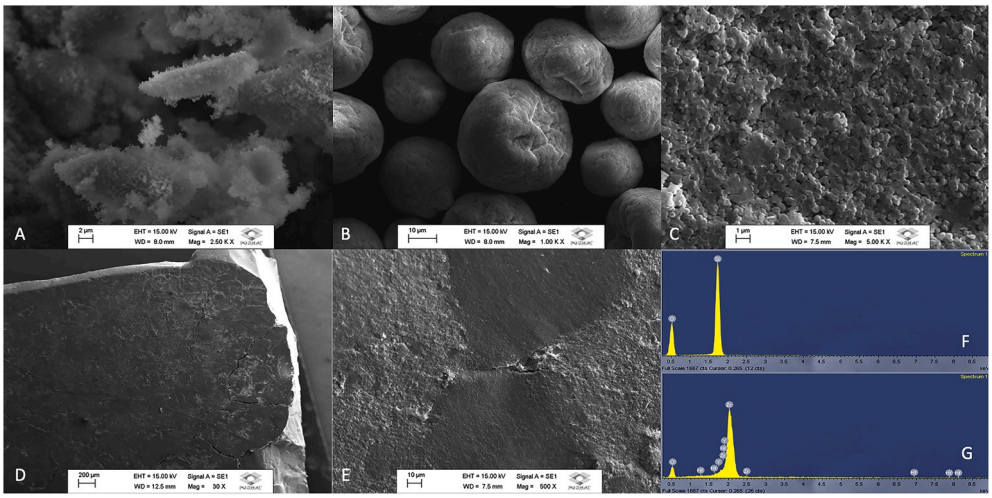

Fig. 2. SEM assessment conducted on the initial silica powder (A); on the Y-TZP initial powder (B) and on a fracture area of a specimen after sintering (C). Pores and cracks can be seen on the fractured area of the specimen (D and E). The EDX analysis was conducted on both silica (F) and Y-TZP (G).

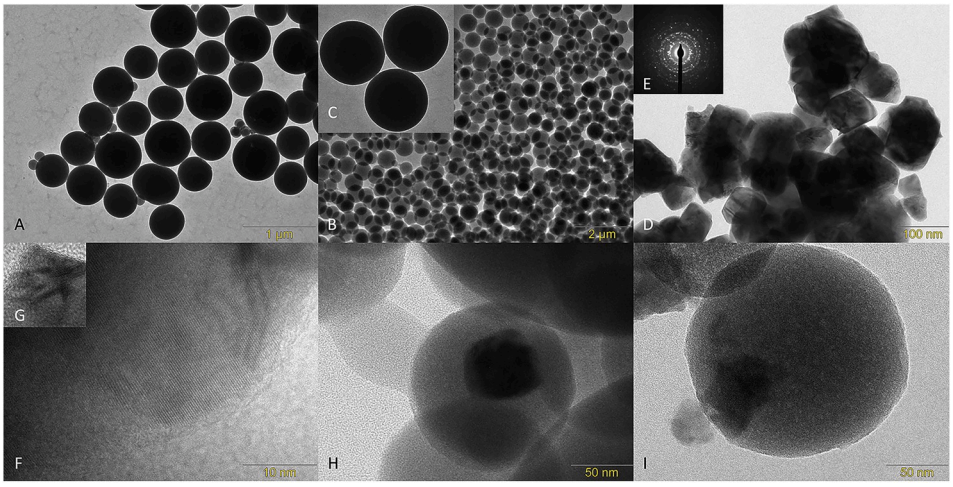

Fig. 3. TEM images of the silica powder in A, B and C, where it can be stated that silica particles were spherical and amorphous due to the lack of a crystallographic pattern. In D, E, F and G the images obtained by the analysis of Y-TZP. Low-magnification TEM image is seen in D, and in E the corresponding FFT pattern of a single nanoparticle, and the crystallographic pattern of a single nanoparticle in F and G. In H and I, the images were obtained before sintering the material (physical mixture), where the Y-TZP particle can be seen in the silica particle (H and I).

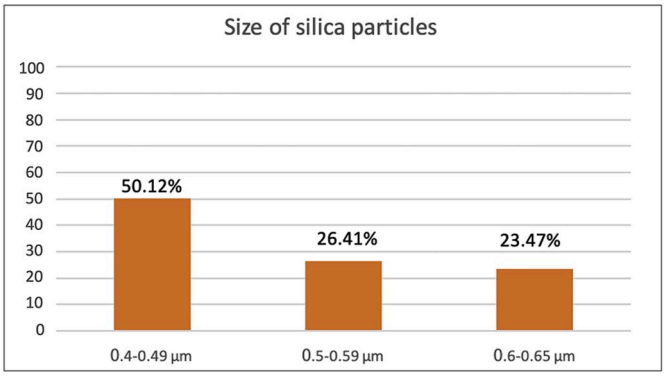

Fig. 4. The TEM images allowed the silica particles to be measured. Most grains of silica (50.12%) was between 0.4 and 0.49 µm, followed by the grains between 0.5 and 0.59 µm (26.41%) and the ones between 0.6 and 0.69 µm (23.47%).

All other peaks related to Y-TZP could not be seen, excepting the ones at 30 and 60°, which are representing the tetragonal allotropic phase of ZrO_2 (Fig. 5).

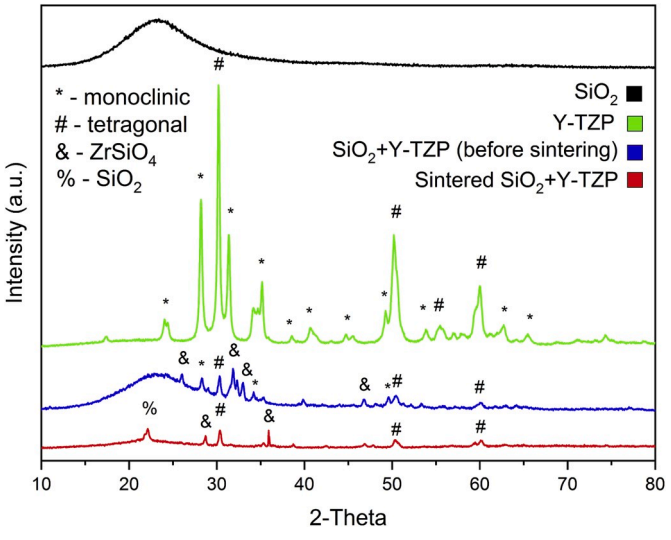

Fig. 5. XRD patterns of the sample before and after sintering at 1150 °C for 2 h (Monoclic zirconia: PDF Card No. 00-001-0750; Tetragonal zirconia: PDF Card No. 00-002-0733; $ZrSiO_4$: PDF Card No. 00-001-0679; SiO_2: PDF Card No. 00-001-0424).

3.4. FTIR

The silica powder and the Y-TZP powders were subjected to analysis by FTIR in order to detect the chemical interactions present in them. Three readings were performed in transmittance mode in each powder, where the band on the axis related to the wave number in cm^{-1} corresponds to a given chemical bond.

The assessment conducted on the silica powder indicated bands at 800 and 961 cm^{-1} assigned to Si–OH groups and a band around 1000-1200 cm^{-1} attributed to the stretching vibration of Si–O–Si bonds (Fig. 6). A delicate band at 1630 cm^{-1} was seen and related to adsorbed H_2O. Also, a band at 2300 cm^{-1} can be assigned to CO_2.

When the Y-TZP was analyzed by FTIR, a broad band at the region of 550–650 cm^{-1} was seen, attributed to the Zr–O bonds (Fig. 6). Smaller bands located between 1000 and 1500 cm^{-1} can be assigned to different organic groups used in the manufacturing process of the Y-TZP powder.

The physical mixture (before sintering) was also subjected to FTIR analysis. This analysis indicated the same bands at the region of 1000–1200 cm^{-1}, 961 cm^{-1} and 800 cm^{-1} attributed to bonds located in the silica powder, and bands in the 550-650 cm^{-1} region related to the Y-TZP powder. Also, the bands at 1630 cm^{-1} and 2300 cm^{-1} associated with adsorbed H_2O and CO_2, respectively. The 1100 cm^{-1} region is also related to the bond related to the interaction of Si and Zr (Si–O–Zr bonds).

After sintering, the bands at 2300 cm^{-1} (CO_2), and at 600-700 cm^{-1} (Zr–O) were maintained. However, those bands located at 1000-12000 cm^{-1} (Si–O–Si), 961 cm^{-1} (Si–OH), were eliminated and that at 550 cm^{-1} lost intensity. The smaller bands located between 1000 and 1500 cm^{-1} were eliminated due to the temperature at which the specimens were subjected during sintering.

3.5. Theoretical density test

The theoretical density value of the experimental ceramics (silica + Y-TZP) was 1.663 g/cm^3.

3.6. Optical properties

3.6.1. CR

The CR measures the transparency or opacity of each material. The EC group showed the highest CR value (more opaque), and it was significantly different from ZLS and LD groups (p = 0,000001). The ZLS group showed the lowest CR value (less opaque), which was different from both LD and EC values. LD showed an intermediate value of CR, and it differed from the values of ZLS and EC (Table 2).

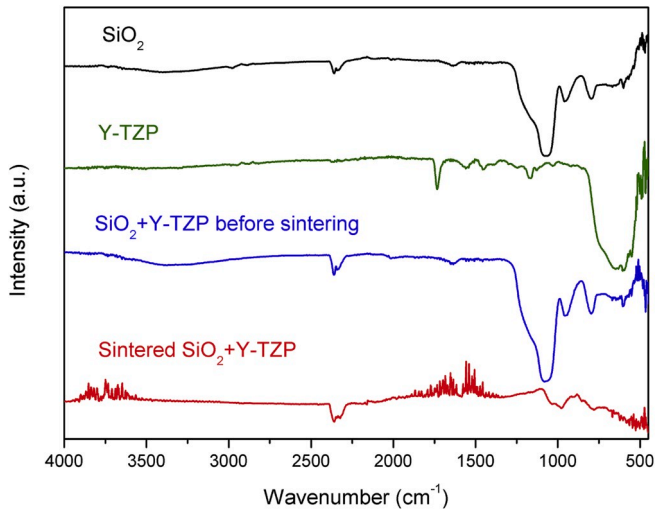

Fig. 6. FTIR spectra of the sample before and after sintering at 1150 °C for 2 h.

3.6.2. TP

The TP measures the masking capacity of each material. Lower ΔE values indicate a better masking capacity. The EC group showed the lowest ΔE value (higher masking capacity), and it was different from both LD and ZLS values (p = 0,000001). The ZLS group showed the highest ΔE value (lower masking capacity), and it was significantly different from LD and EC groups. LD showed an intermediate value of ΔE, and it differed from the values of ZLS and EC.

The medians of CR and ΔE values are displayed in Table 2, along with their interquartile range.

3.7. Mechanical properties

The LD group presented the highest values of flexural strength among all testes materials (p < 0,0001), and it was significantly different from the ZLS and EC, which presented the lowest values of flexural strength and were not significantly different from each other (Table 3).

4. Discussion

This study was able to evidence an alternative method to obtain pure amorphous silica and also evidences an efficient method to synthesize a new glass ceramic containing 97 wt.% silica and 3.0 wt.% Y-TZP. The experimental ceramic presented lower translucency than two commercially available glass-ceramics, but similar flexural strength to one glass-ceramics.

Since its first use (Stöber et al., 1968), the Stöber method has proven to be an efficient route to produce pure, spherical and amorphous silica using tetraethyl orthosilicate (TEOS) as a precursor (Persson et al., 2012; Bangi et al., 2012). These characteristics were confirmed by SEM/EDX, TEM and XRD analyses. Size and shape of silica particles are in accordance with the findings of Buckley and Greenblatt (1994), where ammonia was used as a catalyst (base catalyst), which is responsible for forming larger and more spherical particles/grains than when an acid is used as a catalyst (Stöber et al., 1968). These characteristics are also able to control translucency, homogeneity and the deformation suffered by the specimens during sintering (Jiang et al., 2011; Shui et al., 2002). As also stated in previous studies (Jiang et al., 2011; Pizette et al., 2013), higher green-body strength, better densification and, consequently, improved optical and mechanical properties could be achieved with smaller primary particles.

According to the manufacturer, the Y-TZP powder used in this study was also acquired by a hydrolysis method (TOSOH. Advanced, 2020). Some published studies have already evidence that this route is an alternative to produce Y-TZP materials (Persson et al., 2012; Padovini et al., 2014; Leib et al., 2015). The compounds used in this reaction are not disclosed by the manufacturers, but depending on their composition, it could justify the FTIR bands seen at 1200-1600 cm^{-1} when the Y-TZP powder was analyzed alone. Yet, after sintering, these organic compounds can be eliminated due to the high temperatures at which the material is submitted.

Also, despite the manufacturer stating that the Zpex® is composed only by tetragonal zirconia, the XRD analysis proved that the monoclinic phase is also present. This finding corroborates with the findings of

Table 2
CR and ΔE median ± interquartile range values obtained after statistical analysis.

Group	Contrast Ratio	Translucency parameter (ΔE)
EC	0.999 ± 0.008^{A}	00.165 ± 0.41^{C}
LD	0.752 ± 0.12^{B}	11.485 ± 0.45^{B}
ZLS	0.717 ± 0.22^{C}	13.350 ± 1.05^{A}

*Different capital letters indicate difference between groups (p = 0.000001).

Table 3
Flexural strength values obtained after the statistical analysis.

Group	Flexural Strength (median ± interquartile range)
LD	249.11 ± 49.48[A]
ZLS	105.11 ± 13.70[B]
EC	74.82 ± 8.99[B]

*Different capital letters indicate difference between groups ($p < 0.0001$).

Gauna et al. (2015). However, if this monoclinic phase is metastable, the temperature increase promoted by the sintering protocol could be sufficient to transform this monoclinic zirconia into its tetragonal form. When this reaction happens, during cooling to room temperature, the zirconia does not transform back to the monoclinic state, preserving its tetragonal form and, consequently, its fracture toughness mechanism.

After mixing silica and Y-TZP, a reduction in intensity of the Y-TZP peaks was seen in the XRD patterns. This may be attributed to the proportion of silica/Y-TZP used to prepare the ceramic material. Also, when these two initial powders were mixed and analyzed under TEM, it is possible to observe that the nano-sized ZrO_2 was surrounded by SiO_2 grains. This could also indicate the formation of a Zr–O–Si interlayer, as evidenced by Persson et al. (2012). This interaction between Zr, O and Si would be shown in the FTIR spectra close the 1100 cm^{-1} region regarded as the asymmetric stretching vibration of this bond (Padovini, 2018), yet, due to the intensity of Si–O–Si bonds, seen closely to the same region, this band may not be properly evident.

During mixing, PVB was used as a binding agent in this study. Some studies have also evidenced that the use of a binder may lead to the formation of porosities if not properly eliminated, leading to reduced translucency and strength after sintering (Jiang et al., 2011; Pizette et al., 2013). However, in ambient conditions, the silicon surface is readily covered by oxygen, due to their strong affinity. This makes it difficult to deform these elements and compact then by using a uniaxial/isostatic press without resorting to a binding agent to provide green-body strength (Barraclough et al., 2007). Without a binding agent, the green-body strength of this study's experimental ceramic would rely solely on the van der Waals attraction forces, and could make the compacted specimen susceptible to damage during its removal from the die and handling (Pizette et al., 2013; Barraclough et al., 2007).

The mixture containing silica, Y-TZP and a binding agent was submitted to uniaxial/isostatic powder compressing. This technique has been used to create highly dense and mechanically resistant alternative ceramic materials (Mouzon et al., 2008; Jiang et al., 2011; Lopes et al., 2019). In this study, the experimental ceramic presented lower flexural strength than IPS e.max® CAD and similar value to Celtra Duo®, and lower translucency than IPS e.max® CAD and Celtra Duo®. This finding is in accordance with the study of Mouzon et al. (2008), in which the specimens obtained by the uniaxial/isostatic powder compressing technique presented lower translucency when compared to the slip-casting technique.

After compressing this powder, the green-body specimens were sintered at 1150 °C for 2 h in this study. During the sintering stages, at 600–700 °C the binder is burned out (Baklouti et al., 2001). The increase in the intensity of the FTIR band seen at 2300 cm^{-1} could be attributed to the imprisonment of CO_2 (Sanati and Andersson, 1993) inside the bulk of the material attributed to the evaporation of the binding agent.

Other studies have shown that silica can be compacted at temperatures close to 1250 °C-1300 °C (Barraclough et al., 2007; Santana and Jones, 1996). However, previous studies evidenced that a tetragonal-monoclinic metastable transformation can be seen if zirconia is submitted to temperatures between 1150°C-1200 °C (Persson et al., 2012; Nogami and Tomozawa, 1986). These studies contrast with the findings to this study, once the 1150 °C temperature did not induce the *t-m* phase transformation in zirconia under XDR analysis. Yet, under SEM assessment, it can be seen that the spherical character of silica particles was maintained. This maintenance in the particles shape could also indicate that higher temperature and/or longer periods should be used to promote a better densification of the experimental material. Since no proper densification was achieved with the chosen sintering protocol, the presence of such pores and remaining cracks could have reduced the mechanical and optical properties of the material. Also, due to the high number of pores and cracks on the fracture surface, a fractographic analysis of the origin of the catastrophic failure was unfeasible.

Despite the maintenance of the silica shape, the XRD patterns evidence that this temperature was sufficient to crystallize the amorphous silica particles. Yet, 2 h seem to be insufficient to promote crystal growth, once the intensity of the XDR peak attributed to silica crystallization is quite mild. These findings corroborate to the study of Persson et al. (2012), in which SiO_2–ZrO_2 ceramics were submitted to either 10 or 15-h sintering stages, and it resulted in more intense silica XRD peaks, in spite of the percentage of silica being smaller than in this study.

Nonetheless, in the study conducted by Jiang et al. (2011), Y-TZP specimens were sintered for 2 h and translucency was achieved even for primary particles over 40 nm. It points out that primary particles size and temperature of sintering are important factors to be taken into account in order to achieve proper translucency (Jiang et al., 2011). In this study, however, the temperature used is lower than in Jiang's study, which could be held responsible for the lower densification and, consequently, lower translucency obtained for the experimental ceramic. In this present study, the residual porosity could be responsible for the lack of translucency, once the difference in the refractive indexes between the grains of SiO_2 and air inside the pores could have made light to scatter through the material (Jiang et al., 2011; Heffernan et al., 2001; Peelen and Metselaar, 1974). Thus, since the amount of light that was transmitted, absorbed and reflected was disturbed by these different refractive indexes, the material looked opaque.

In view of what has been discussed, the use of a binding agent associated with short sintering period and lower temperatures could have resulted in a high level of porosities, which hindered the translucency of the experimental material. Yet, it is important to highlight that this study contributes to the scientific literature by evidencing that the uniaxial/isostatic powder compression is an efficient processing method of experimental ceramics with dental purposes.

Further studies are necessary to investigate if different sintering protocols are sufficient to eliminate the pores of this material even in the presence of a binding agent and promote crystal growth and better translucency. Also, if these higher temperatures are tested, the *t-m* metastable transformation should also be analyzed, associated with different mechanical tests (e.g. biaxial flexural strength and fracture toughness tests) in order to properly evaluate the sintering consequences in the material's physical and mechanical properties in order for it to be used as an alternative dental ceramic.

5. Conclusion

Within the limitations of this study, it can be concluded that the uniaxial/isostatic powder compression is an efficient method to obtain experimental ceramics for dental purposes. Also, 1150 °C for 2 h is sufficient to crystallize SiO_2 without inducing t-m transformation of zirconia. Yet, this sintering protocol seems to be insufficient to densify the experimental ceramic, which consequently resulted in reasonable flexural strength, but higher contrast ratio and lower translucency parameter when compared to lithium disilicate and zirconia-reinforced lithium silicate. Further studies with different sintering protocols are needed in order to properly achieve a good balance between optical and mechanical properties for this experimental material.

Author contributions

Victor Mosquim: Conceptualization, Methodology, Validation, Formal analysis, Investigation, Resources, Writing - Original Draft,

Writing - Review & Editing, Visualization, Funding acquisition.

Brunna Mota Ferrairo: Methodology, Validation, Investigation, Resources, Writing - Review & Editing, Visualization.

Mariele Vertuan: Investigation, Resources, Writing - Review & Editing.

Aroldo Geraldo Magdalena: Conceptualization, Methodology, Validation, Investigation, Resources, Writing - Review & Editing, Visualization, Project administration.

Carlos Alberto Fortulan: Conceptualization, Methodology, Validation, Investigation, Resources, Writing - Review & Editing, Project administration.

Paulo Noronha Lisboa Filho: Conceptualization, Methodology, Validation, Resources, Writing - Review & Editing, Project administration.

Paulo Francisco Cesar: Methodology, Validation, Resources, Writing - Review & Editing, Project administration.

Estevam Augusto Bonfante: Methodology, Validation, Resources, Writing - Review & Editing, Project administration.

Heitor Marques Honório: Validation, Resources, Writing - Review & Editing.

Ana Flávia Sanches Borges: Conceptualization, Methodology, Validation, Formal analysis, Resources, Writing - Original Draft, Writing - Review & Editing, Visualization, Supervision, Project administration, Funding acquisition.

Declaration of competing interest

The authors declare that they have no known competing financial interests or personal relationships that could have appeared to influence the work reported in this paper.

Acknowledgements

Funding: This study was financed by São Paulo Research Foundation (FAPESP, #2017/18157-4). This study was financed in part by the Coordenação de Aperfeiçoamento de Pessoal de Nível Superior - Brasil (CAPES) - Finance Code 001. These funding sources had no involvement in the study design; in the collection, analysis and interpretation of data; in the writing of the manuscript; and in the decision to submit the article for publication.

References

Baklouti, S., Bouaziz, J., Chartier, T., Baumard, J., 2001. Binder burnout and evolution of the mechanical strength of dry-pressed ceramics containing poly(vinyl acohol). J. Eur. Ceram. Soc. 21, 1087–1092. https://doi.org/10.1016/S0955-2219(00)00305-8.

Bangi, U.K.H., Park, C., Baek, S., Park, H., 2012. Improvement in optical and physical properties of TEOS based aerogels using acetonitrile via ambient pressure drying. Ceram. Int. 38, 6883–6888. https://doi.org/10.1016/j.ceramint.2012.07.051.

Barraclough, K.G., Loni, A., Caffull, E., Canham, L.T., 2007. Cold compaction of silicon powders without a binding agent. Mater. Lett. 61, 485–487. https://doi.org/10.1016/j.matlet.2006.04.102.

Brodbelt, R.H.W., O'Brien, W.J., Fan, P.L., 1980. Translucency of dental porcelains. J. Dent. Res. 59, 70–75. https://doi.org/10.1177/00220345800590011101.

Buckley, A.M., Greenblatt, M., 1994. The sol-gel preparation of silica gels. J. Chem. Educ. 71, 599–602. https://doi.org/10.1021/ed071p599.

Chavalier, J., Gremillard, L., Deville, S., 2007. Low-temperature degradation of zirconia and implications for biomedical implants. Annu. Rev. Mater. Res. 37, 1–32. https://doi.org/10.1146/annurev.matsci.37.052506.084250.

Chu, F.C., Chow, T.W., Chai, J., 2007. Contrast ratios and masking ability of three types of ceramic veneers. J. Prosthet. Dent 98, 359–364. https://doi.org/10.1016/S0022-3913(07)60120-6.

Della Bona, A., Nogueira, A.D., Pecho, O.E., 2014. Optical properties of CAD-CAM ceramic systems. J. Dent. 42, 1202–1209. https://doi.org/10.1016/j.jdent.2014.07.005.

dos Santos, D.M., da Silva, E.V.F., Watanabe, D., Bitencourt, S.B., Guiotti, A.M., Goiato, M.C., 2017. Effect of different acidic solutions on the optical behavior of lithium disilicate ceramics. J. Prosthet. Dent 118, 430–436. https://doi.org/10.1016/j.prosdent.2016.10.023.

El-Gahny, O.S.A., Sherief, A.H., 2016. Zirconia based ceramics, some clinical and biological aspects: review. Future Dent. J. 2, 55–64. https://doi.org/10.1016/j.fdj.2016.10.002.

Gauna, M.R., Conconi, M.S., Gomez, S., Suarez, G., Aglietti, E.F., Rendtorff, N.M., 2015. Monoclinic - tetragonal zirconia quantification of commercial nanopowder mixtures by XRD and DTA. Ceram-Silikáty 59, 318–325.

Guazzato, M., Albakry, M., Ringer, S.P., Swain, M.V., 2004. Strength, fracture toughness and microstructure of a selection of all-ceramic materials. Part II. Zirconia-based dental ceramics. Dent. Mater. 20, 449–456. https://doi.org/10.1016/j.dental.2003.05.002.

Hanawalt, J.D., Rinn, H.W., Frevel, L.K., 1938. Chemical analysis by X-Ray diffraction. Indust. Chem. Anal. Ed. 10, 475–512. https://doi.org/10.1021/ac50125a001.

Heffernan, M.J., Aquilino, S.A., Diaz-Arnold, A.M., Haselton, D.R., Stanford, C.M., Vargas, M.A., 2001. Relative translucency of six all-ceramic systems. Part I: core materials. J. Prosthet. Dent 88, 4–9. https://doi.org/10.1067/mpr.2002.126794.

Jiang, L., Liao, Y., Wan, Q., Li, W., 2011. Effects of sintering temperature and particle size on the translucency of zirconium dioxide dental ceramic. J. Mater. Sci. Mater. Med. 22, 2429–2435. https://doi.org/10.1007/s10856-011-4438-9.

Kelly, J.R., 2008. Dental ceramics: what is this stuff anyway? J. Am. Dent. Assoc. 139, 4S–7S. https://doi.org/10.14219/jada.archive.2008.0359.

Kelly, J.R., Benetti, P., 2011. Ceramic materials in dentistry: historical evolution and current practice. Aust. Dent. J. 56, 84–96. https://doi.org/10.1111/j.1834-7819.2010.01299.x.

Kelly, J.R., Denry, I., 2008. Stabilized zirconia as a structural ceramic: an overview. Dent. Mater. 24, 289–298. https://doi.org/10.1016/j.dental.2007.05.005.

Leib, E.W., Vainio, U., Pasquarelli, R.M., Kus, J., Czaschke, C., Walter, N., Janssen, R., Müller, M., Schreyer, A., Weller, H., Vossmeyer, T., 2015. Synthesis and thermal stability of zirconia and yttria-stabilized zirconia microspheres. J. Colloid Interface Sci. 448, 582–592. https://doi.org/10.1016/j.jcis.2015.02.049.

Liu, J., Cao, L., Huang, J., Xin, Y., Yang, W., Fei, J., Yao, C., 2012. A ZrSiO4/SiC oxidation protective coating for carbon/carbon composites. Surf. Coating. Technol. 206, 3270–3274. https://doi.org/10.1016/j.surfcoat.2012.01.030.

Lopes, A.C.O., Coelho, P.G., Witek, L., Benalcázar Jalkh, E.B., Gênova, L.A., Monteiro, K. N., Cesar, P.F., Lisboa Filho, L.F., Bergamo, E.T.P., Ramalho, I.S., Bonfante, E.A., 2019. Nanomechanical and microstructural characterization of a zirconia-toughened alumina composite after aging. Ceram. Int. 45, 8840–8846. https://doi.org/10.1016/j.ceramint.2019.01.211.

McCabe, J.F., Walls, A.W.G., 2008. Ceramics and porcelain fused to metal (PFM). In: McCabe, J.F., Walls, A.W.G. (Eds.), Applied Dental Materials. Oxford University Press, Oxford, pp. 89–100.

Mouzon, J., Glowacki, E., Odén, M., 2008. Comparison between slip-casting and uniaxial pressing for the fabrication of translucent yttria ceramics. J. Mater. Sci. 43, 2849–2856. https://doi.org/10.1007/s10853-007-2261-y.

Nogami, M., Tomozawa, M., 1986. ZrO_2-transformation-toughened glass-ceramics prepared by the sol-gel process from metal alkoxides. J. Am. Ceram. Soc. 69, 99–102. https://doi.org/10.1111/j.1151-2916.1986.tb04709.x.

Nogueira, A.D., Della Bona, A., 2013. The effect of a coupling medium on color and translucency of CAD-CAM ceramics. J. Dent. 41, e18–e23. https://doi.org/10.1016/j.jdent.2013.02.005.

Padovini, D.S.S., 2018. *Estudo de adsorção e fotodegradação da rodamina b com nanopartículas core-shell de ZrO_2@SiO_2 preparadas pelo método sol-gel*. University of the State of São Paulo-UNESP, São Paulo. Dissertation (Master in Materials Science) – School of Science.

Padovini, D.S.S., Pontes, D.S.L., Dalmaschio, C.J., Pontes, F.M., Longo, E., 2014. Facile synthesis and characterization of ZrO2 nanoparticles prepared by the AOP/hydrothermal route. RSC Adv. 4, 38484–38490. https://doi.org/10.1039/C4RA04861J.

Peelen, J.G.J., Metselaar, R., 1974. Light scattering by pores in poly-crystalline materials. J. Appl. Phys. 45, 216–220. https://doi.org/10.1063/1.1662961.

Persson, C., Unosson, E., Ajaxon, I., Engstrand, J., Engqvist, H., Xia, W., 2012. Nano grain sized zirconia–silica glass ceramics for dental applications. J. Eur. Ceram. Soc. 32, 4105–4110. https://doi.org/10.1016/j.jeurceramsoc.2012.06.028.

Pizette, P., Martin, C.L., Delette, G., Sans, F., Geneves, T., 2013. Green strength of binder-free ceramics. J. Eur. Ceram. Soc. 33, 975–984. https://doi.org/10.1016/j.jeurceramsoc.2012.11.018.

Ramos, C.M., Tabata, A.S., Cesar, P.F., Rubo, J.H., Fracisconi, P.A., Sanches Borges, A.F., 2015. Application of micro-Raman spectroscopy to the study of yttria-stabilized tetragonal zirconia polycrystal (Y-TZP) phase transformation. Appl. Spectrosc. 69, 810–814. https://doi.org/10.1366/14-07793.

Riquieri, H., Monteiro, J.B., Viegas, D.C., Campos, T.M.B., de Melo, R.M., de Siqueira Ferreira Anzaloni Saavedra, G., 2018. Impact of crystallization firing process on the microstructure and flexural strength of zirconia-reinforced lithium silicate glass-ceramics. Dent. Mater. 34, 1483–1491. https://doi.org/10.1016/j.dental.2018.06.010.

Ruff, O., Ebert, F., Stephan, E., 1929. Beitrage zur keramik hochfeurfe stoffe II. Das system ZrO2-CaO. Z. Anorg. Allg. Chem. 180, 215–224.

Sanati, M., Andersson, A., 1993. DRIFT study of the oxidation and the ammoxidation of toluene over a TiO_2 (B) -supported vanadia catalyst. J. Mol. Catal. 81, 51–62. https://doi.org/10.1016/0304-5102(93)80022-M.

Santana, C.J., Jones, K.S., 1996. The effects of processing conditions on the density and microstructure of hot-pressed silicon powder. J. Mater. Sci. 31, 4985–4990. https://doi.org/10.1007/BF00355891.

Shui, A., Kato, Z., Tanaka, S., Uchida, N., Uematsu, K., 2002. Sintering deformation caused by particle orientation in uniaxially and isostatically pressed alumina compacts. J. Eur. Ceram. Soc. 22, 311–316. https://doi.org/10.1016/S0955-2219(01)00292-8.

Stöber, W., Fink, A., Bohn, E., 1968. Controlled growth of monodisperse silica spheres in the micron size range. J. Colloid Interface Sci. 26, 62–69. https://doi.org/10.1016/0021-9797(68)90272-5.

TOSOH. Advanced. Ceramics | zirconia powders. accessed March 9th, 2020. https://www.tosoh.com/our-products/advanced-materials/zirconia-powders.
Volpato, C.A.M., Garbelotto, L.G.D., Fredel, M.C., Bondioli, F., 2011. Application of zirconia in dentistry: biological, mechanical and optical considerations. In: Sikalidis, C. Advances in Ceramics: Electric and Magnetic Ceramics, Bioceramics, Ceramics and Environment. IntechOpen, London, pp. 397–420.
Wyckoff, R.W.G., 1925. Crystal structure of high temperature cristobalite. Am. J. Sci. 9, 448–459. https://doi.org/10.2475/ajs.s5-9.54.448.